J Mater Sci (2009) 44:689–699
DOI 10.1007/s10853-008-3202-0

Pore evolution model of ceramic membrane during constrained sintering

Minghui Qiu · Jun Feng · Yiqun Fan · Nanping Xu

Received: 8 August 2008 / Accepted: 17 December 2008 / Published online: 13 January 2009

Abstract Pore size has been found to strongly depend on the sintering program in the preparation of porous ceramic membranes. In this paper, a model was developed to predict the variation in pore size and porosity of membranes during the sintering process. A comparison of shrinkage characteristics was made between the sintering processes of supported membranes and unsupported membranes. For supported membranes, the effect of restriction coming from a rigid substrate on the sintering behavior has been taken into account in the calculation. It is predicted that the pore size increases in supported membranes and decreases in unsupported membranes as the sintering temperature is increased. Calculations also showed that the loss of porosity in the supported membranes was less than that in the unsupported membranes. In order to verify reliability of this model, unsupported and supported membranes were prepared with α-Al_2O_3 powders at the sintering temperatures ranging from 1125 °C to 1325 °C. The pore size and porosity were measured by gas permeation technique and Archimedes's method. The experimental results for the unsupported and supported α-Al_2O_3 membranes showed a good agreement with those calculated from the model. Therefore, this model provides an effective tool in predicting the porosity and the pore size of ceramic membranes at the different sintering temperatures.

M. Qiu · J. Feng · Y. Fan (✉) · N. Xu
State Key Laboratory of Materials-Oriented Chemical Engineering, College of Chemistry and Chemical Engineering, Nanjing University of Technology, Nanjing 210009, China
e-mail: yiqunfan@njut.edu.cn

Introduction

Ceramic membranes possess some inherent advantages over the organic ones, such as superior thermal and mechanical stabilities, chemical and microbiological resistance, and long life [1]. These merits make them competitive when used at high temperatures and in harsh chemical environments. Asymmetric ceramic membranes with the structure of a thin separation layer and a porous support are widely employed in separation processes due to their outstanding mechanical strength and permeation flux [2, 3]. The membranes are generally prepared by solid-state sintering at a high temperature to produce sufficient strength and required pore morphology [2, 4]. The final microstructure such as pore size, porosity, and tortuosity are closely related to the parameters of the sintering processing including temperature, pressure, particle size, green density, which have been studied widely [5–7]. The work of sintering additives has also been performed on microstructure control in ceramics [7–9]. Harmer and coworkers [10] performed work on both microstructural evolution during sintering and the optimization of processing and microstructures through the use of additives. The support, sintered at temperatures higher than the sintering temperature of the membrane layer, serves as a rigid substrate allowing the membrane layer to shrink only in the direction perpendicular to the surface. This restriction is also found to affect membrane microstructure during the sintering process [11–14]. Wang et al. [11] discovered that there was an obvious difference in the pore size changes between supported and unsupported membranes. Levänen and Mäntylä [12] demonstrated that the pore size was almost unchanged on unsupported membranes when changing the sintering temperature from 1200 to 1400 °C, while a significant increment was found on α-alumina supported

membranes during the sintering temperature range. Shojai and Mäntylä [2] pointed out that as the sintering temperature was increased from 1000 °C to 1200 °C, the trends for pore size variation were different between unsupported and supported 3Y-ZrO_2 membranes. These experimental observations have confirmed the significant contribution of rigid substrates to membrane pore size formed in the sintering process.

The sintering of thin films on rigid substrates is of relevance to the general problem of constrained sintering, which has been researched in many fields such as ceramic membranes [15], multilayer electronic packages, especially low-temperature co-fired ceramics (LTCC) [16], and solid oxide fuel cells (SOFC) [17]. Constrained sintering involves the use of nonsintering layers, either porous or fully dense, to constrain the shrinkage in the layer plane. It means sintering shrinkage is precisely controlled and tolerances are more easily kept within the plane when multiple layers are sintered. Since the 1980s, fundamental studies of how the constraint works and effect on the densification process has been modeled in several literatures [18–23]. Scherer and Garino [19] found that the substrate exerted a tensile stress on the porous glass layer and predicted the magnitude of this stress. Moreover, Garino and Bowen [20] studied the densification kinetics of constrained films in the case of viscous sintering. Bordia and Raj [21] modeled the sintering behavior of a constrained film supported by a rigid substrate. They simplified the case by assuming that the stress field developed in the film was uniform. Carroll and Rahaman [22] developed a physical model that assumed uniform, simple cubic packing of spherical particles for the initial stage sintering in the case of a constrained thin film. These models focused on the tensile stress exerted by the substrate and its effect on the densification and the formation of defects. However, these models cannot accurately describe the sintering of porous ceramic membranes on macroporous supports. Further quantitative evaluation of pore size and porosity in the membranes has not been performed to our best knowledge.

Based on constrained sintering theory, this paper aims to propose a model to quantitatively describe the dependence of pore size and porosity of supported membranes on the sintering temperature. Experimental investigations of pore size and porosity have been conducted to verify the reliability of the proposed model.

Mechanism and modeling of constrained sintering

Solid-state sintering process is usually divided into three stages: (1) formation of necks between spherical particles, (2) transient state from porous structure to dense structure, and (3) formation of dense structure. The process of membrane sintering is considered to occur at the initial stage as typically described by a simple two-particle model [24]. The model treated ceramic particles as spheres with the uniform size, and assumed neck formation and growth by material transport. The dominant transport mechanism, however, can vary depending on particle size, neck radius, temperature, and time for a given system. There are at least six different transport mechanisms in materials sintering for a system of two sintering particles [25]. Some of these material transport mechanisms contribute to shrinkage (Fig. 1a) while others do not (Fig. 1b). When the non-densifying mechanisms occur, the sintering driving force may be reduced due to vacancy absorption at grain boundaries. It will result in reducing the sintering rate. However, this contribution is low compared and not usually considered during the sintering process of membranes. In the case of unconstrained sintering, any particle displacement is not restricted as long as mass transport over distances comparable to the particle size. That is "shrinkage" in all three directions occurs since the centers of the spheres get closer together as a result of no constraint, as

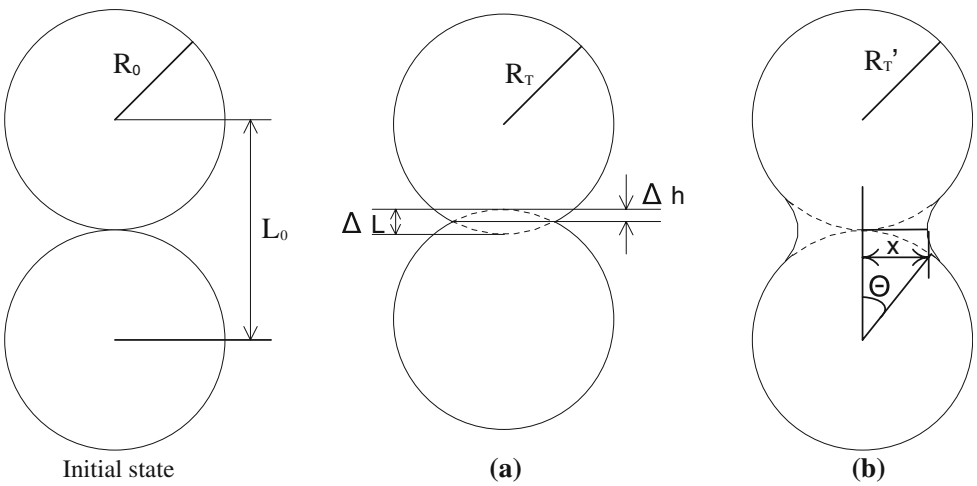

Fig. 1 Two-particle model for initial stage sintering **a** with shrinkage and **b** without shrinkage

shown in Fig. 1a. For constrained sintering of supported membranes, however, the shrinkage in x–y directions is fully restricted by the porous substrate, resulting in unchanged interparticle distance but increased neck size due to mass transport. The results are in agreement with the case shown in Fig. 1b.

In order to discuss the evolution mechanism of pore size, simplifications were made as follows:

(1) The material is composed of spherical particles with uniform radius, denoted by R;
(2) The pores are cylindrical in shape, $d_p = 4V/A$ [26], where V and A are the pore volume per weight and the specific surface area, respectively;
(3) The coordination number of each particle is c for both unsupported and supported membranes. When $c = 6$, particles stack in a simple cubic array, as shown in Fig. 2;
(4) Unsupported membranes are bulk green bodies and sintered fully isotropic in all dimensions;
(5) Supported membranes consist of multilayer identical cylindrical particles, each having an identical number of neighbors no matter where the particle stacks in pore or surface of the support;
(6) The thickness of the membrane are much smaller than the in-plane dimensions, and the misfit stresses generated in the membrane when it sinters could be assumed to be uniform through the thickness;
(7) Initial-stage solid sintering involves neither a phase transition nor a reaction.

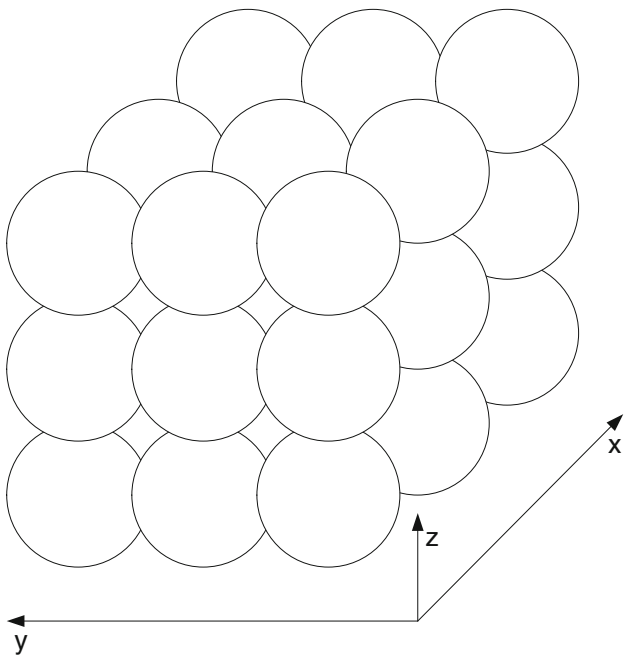

Fig. 2 Particles stacked in a simple cubic array

The above assumptions can be justified if sintering is homogeneous. Real samples may show local shrinkage inhomogeneity due to void space, zones of nonuniform particle packing, and agglomerates. Although this inhomogeneity could induce deviation between predicted results and experimental data when the model used to actual system, the model with consideration of the 3D geometry influence is helpful to predict the pore size variation for the support membrane during the constrained sintering process.

Description of constrained sintering of supported membrane

During sintering, the membrane is usually heated up to a temperature at which necks are formed to provide sufficient strength and necessary pore structure [2, 4]. The microstructure of ceramic membranes, therefore, is affected by the sintering temperature. If the sintering process is unconstrained, membrane shrinkage occurs in all three directions as sintering temperature increases (Fig. 3a). Furthermore, the degree of shrinkage at the three directions is almost the same, that is, $\varepsilon_x = \varepsilon_y = \varepsilon_z = \varepsilon_{free}$. Based on the two-particle model, the shrinkage is caused by neck growth with centers of the spheres getting closer (Fig. 1a), results in continuous shrinkage of the pore size [2].

For a supported membrane, as the porous alumina support has been sintered at higher than 1650 °C, it acts as rigid structure and eliminates the shrinkage in the x–y directions of the membrane layer during the sintering process. The actual supports are different from rigid dense support described in most constrained models [18–21] in the following ways. For one thing, the porosity of the support (φ_s) will decrease the contact areas of the support with the particles deposited on by a factor of $(1 - \varphi_s)$. For another, surface roughness of the support may increase the number of contacts and the contact areas because rough surfaces have larger areas compared to smooth surfaces. However, unless the cracking and curling occur, the shrinkage in x–y directions of the membrane layer is fully constrained by such rigid support of zero-shrinkage ($\varepsilon_x = \varepsilon_y = 0$) (Fig. 3b) due to the in-plane tensile stress, (σ_x, σ_y), which arises from the interfacial friction between constrained and releasing layers [21, 27–30]. Accordingly, for the constrained sintering of supported membrane, the model shown in Fig. 1b can be applied to describe the shrinkage in x–y direction, where the spheres cannot move freely; while the model shown in Fig. 1a can be used for z direction shrinkage, in which the sphere centers get closer. In-plane tensile stress exerted by the substrate can change the pore structure and lend to differences in pore evolution compared with the free sintering. Meanwhile, the thickness

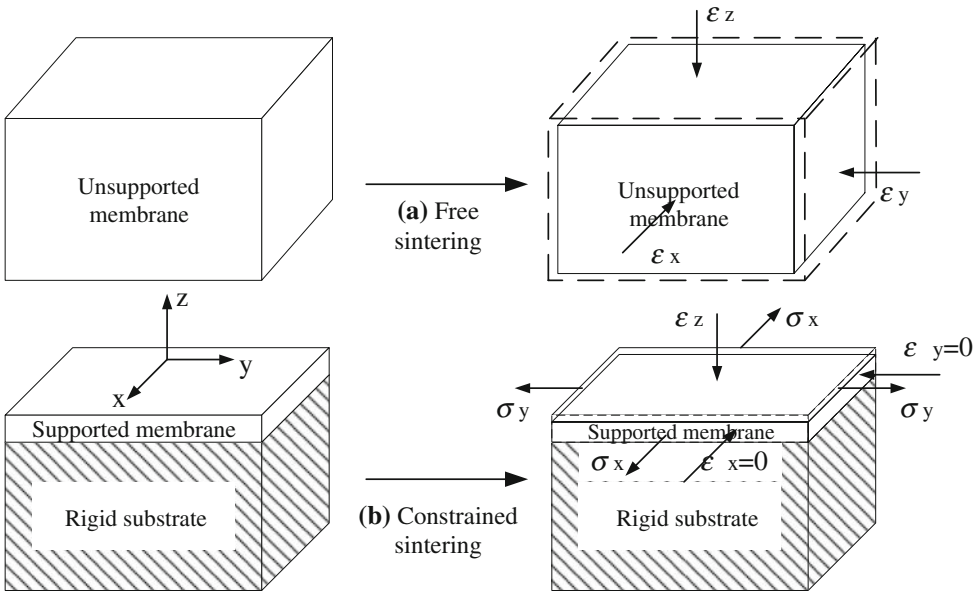

Fig. 3 Sketch map of **a** free sintering and **b** constrained sintering

of the membrane will decrease due to shrinkage in the z-direction.

Modeling of pore growth for constrained sintering

Based on the assumption (3), if the coordination number of each particle is c, each sphere is in contact with c ones under the stacking state. The porosity (φ_0), the pore volume per weight (V_0), and the specific surface area (A_0) in the initial stacking state can then be calculated from the following equations:

$$1-\varphi_0=\frac{\frac{1}{(2R_0)^3}\times\frac{4}{3}\pi R_0^3}{1}=\frac{\pi}{6} \tag{1}$$

$$V_0=\frac{\varphi_0}{\rho(1-\varphi_0)} \tag{2}$$

$$A_0=\frac{\frac{1}{\rho}\times 4\pi R_0^2}{\frac{4}{3}\pi R_0^3}=\frac{3}{\rho R_0} \tag{3}$$

where ρ is the density of alumina, and R_0 is the particle radius.

In the case of unconstrained sintering process, shrinkage occurs in three directions (Fig. 3a). The density of the solid material is constant, thus mass conservation requires that the volume of solid material remains constant during the sintering process. There should be a balance according to Eq. 4.

$$\frac{4}{3}\pi R_T^3-c\cdot\pi\Delta h^2\cdot\left(R_T-\frac{\Delta h}{3}\right)=\frac{4}{3}\pi R_0^3 \tag{4}$$

From Eq. 4, the normal radius can be calculated by Eq. 5 when the sintering temperature is T.

$$R_T^3=\frac{4R_0^3}{4-3cP^2+cP^3} \tag{5}$$

where $P=\frac{\Delta h}{R_T}$, $\Delta h=(\Delta L/L_0)\cdot R_0$, which is the shrinkage between the centers of two particles. Furthermore, the porosity, pore volume per weight, and specific surface area after sintering at temperature T can be calculated from Eqs. 6, 7, and 8, respectively:

$$\varphi_T=1-\frac{\frac{V_0}{\varphi_0}(1-\varphi_0)}{\frac{V_0}{\varphi_0}(1-\frac{\Delta L}{L_0})^3}=1-\frac{1-\varphi_0}{(1-\frac{\Delta L}{L_0})^3} \tag{6}$$

$$V_T=\frac{\varphi_T}{\varphi_0}\cdot\frac{1-\varphi_0}{1-\varphi_T}\cdot V_0 \tag{7}$$

$$A_T=\frac{\frac{1}{\rho}\cdot(4\pi R_T^2-c\cdot 2\pi R_T\Delta h)}{\frac{4}{3}\pi R_T^3} \tag{8}$$

where $\Delta L/L_0$ is the shrinkage that can be measured by means of a dilatometer. Combining Eqs. 7 and 8, the pore size after sintering can be deduced from Eq. 9:

$$d_p=\frac{4V_T}{A_T}=\frac{\frac{4}{3}R_T^2\cdot\frac{\varphi_T}{1-\varphi_T}}{R_T-\frac{c}{2}\cdot\Delta h} \tag{9}$$

For the supported membrane, shrinkage is constrained by the rigid porous substrate and can only occur in the z-direction (Fig. 3b). Therefore, according to the conservation of the solid volume, we have Eq. 10:

$$\frac{4}{3}\pi R_T'^3-\frac{c}{3}\cdot\pi\Delta h^2\cdot\left(R_T'-\frac{\Delta h}{3}\right)=\frac{4}{3}\pi R_0^3 \tag{10}$$

Thus, after constrained sintering, the normal radius and the porosity caused by one-dimensional shrinkage will be governed by Eqs. 11 and 12, respectively:

$$R_T'^3 = \frac{4R_0^3}{4 - cP^2 + \frac{c}{3}\cdot P^3} \tag{11}$$

$$\varphi_T' = 1 - \frac{\frac{V_0}{\varphi_0}(1-\varphi_0)}{\frac{V_0}{\varphi_0}\left(1-\frac{\Delta L}{L_0}\right)} = 1 - \frac{1-\varphi_0}{1-\frac{\Delta L}{L_0}} \tag{12}$$

Substituting Eq. 12 into Eq. 7, pore volume per weight can be calculated by Eq. 13. It becomes that the degree of pore volume diminution on the supported membrane is lower than that on the unsupported membrane. Meanwhile, the tensile stress caused by shrinkage limitation could decrease sintering driving force, and make the surface area variation less than unsupported membrane. Based on geometric relationship, specific surface area after constrained sintering can be calculated by Eq. 14. The reduction of specific surface area is caused by both shrinkage in z-direction (Fig. 1a) and mass transport from the convex regions to the concave regions between particles in x–y direction (Fig. 1b) [26].

$$V_T' = \frac{\varphi_T'}{\varphi_0}\cdot\frac{1-\varphi_0}{1-\varphi_T'}\cdot V_0 = \frac{\varphi_T'}{\rho(1-\varphi_T')} \tag{13}$$

$$A_T' = \frac{\frac{1}{\rho}\cdot\left\{4\pi R_T'^2 - \frac{c}{3}\cdot 2\pi R_T'\Delta h - \frac{2c}{3}\times\left[2\pi R_T'^2(1-\cos\theta) - \frac{\pi^2 x^3}{2R_T'}\right]\right\}}{\frac{4}{3}\pi R_T'^3} \tag{14}$$

$$\cos\theta = \frac{R_T' - \Delta h}{R_T'} \quad \text{and}$$

$$x = \sqrt{R_T'^2 - (R_T' - \Delta h)^2} = R_T'\sin\theta$$

Combining Eqs. 13 and 14, the pore size of supported membrane after constrained sintering can be deduced from Eq. 15:

$$d_p' = \frac{\frac{4}{3}R_T'^2\cdot\frac{\varphi_T'}{1-\varphi_T'}}{R_T' - \frac{c}{2}\cdot\Delta h + \frac{c\cdot\pi}{12}R_T'\sin^3\theta} \tag{15}$$

Though the actual membranes are staked more random than such simple stack described by above model, and the membrane may be too thick to generate stresses uniformly through the thickness dimension, the effect of restriction coming from a rigid substrate on the sintering behavior and pore evolution have been taken into account in the model above.

Experimental

Materials and membrane preparation

The membranes were prepared on inner surface of porous tubular α-alumina supports by dip-coating method. The supports have the dimensions of 12 mm in outer diameter, 2 mm in wall thickness, 85 mm in length, and 2.4 μm in mean pore diameter. The coating slurry contained α-alumina powders (average particle size of 0.45 μm) with the solid content of 10 wt%. The α-alumina powders were dispersed in pure water with nitric acid as a dispersant and stirred for 120 min. Methylcellulose (MC) was used as a binder to add to the slurry. The resulting mixture was stirred for 30 min. To achieve complete dispersion, the slurry was further treated in ultrasonic for 10 min before used for coating. Then the treated support was dipped into the slurry for 60 s to form the supported membranes with the thickness of 20 μm. The porosity and roughness of alumina porous supports were 33–35% and 2–3 μm, respectively. Thus, the supported membranes with the thickness of 20 μm were thick enough to cover the porous support completely. Moreover, in order to preclude infiltration of particles into the porous support, the polymeric compound (MC) was added to the slurry to determine the viscosity and increase the attractive force between all the alumina particles. As a result, particles contacted spontaneously and stacked on the surface of support. Each particle contacted with neighboring ones by neck connection, until it was affected by support indirectly. There were no sliding and no cracking for membranes on the support during the sintering process, then at the macroscopic scale, the shrinkage in x–y directions of the membrane layer was fully constrained by such rigid support of zero-shrinkage.

For comparison, unsupported membranes were prepared by dry pressing. The slurry described above was heated at 120 °C until dried out. The achieved powders were milled and sieved by an 80-mesh screen. The particles were then pressed into unsupported disk membranes with the diameter of 30 mm and the thickness of 2.5 mm.

Both the supported and unsupported membranes were initially dried at 70 °C for 10 h and then at 120 °C for 10 h. The dried membranes were sintered, respectively, at 1125, 1175, 1225, 1275, and 1325 °C for 2 h. The heating rate was controlled at 2 °C/min. Figure 4 gives the SEM image of cross-section of Al_2O_3 supported membrane sintered at 1225 °C. It illustrates the excellent interface with no obviously penetration between membrane layer and support. And the neck contact between particles of membrane can be demonstrated obviously.

Dilatometry

The shrinkage of the unsupported membranes was measured by means of a dilatometer (Netzsch DIL 402C, Germany). The measured sample was the "green" unsupported membrane with the dimensions of 2.5 × 2.5 × 2.5 mm^3. Shrinkage measurements at a constant rate of

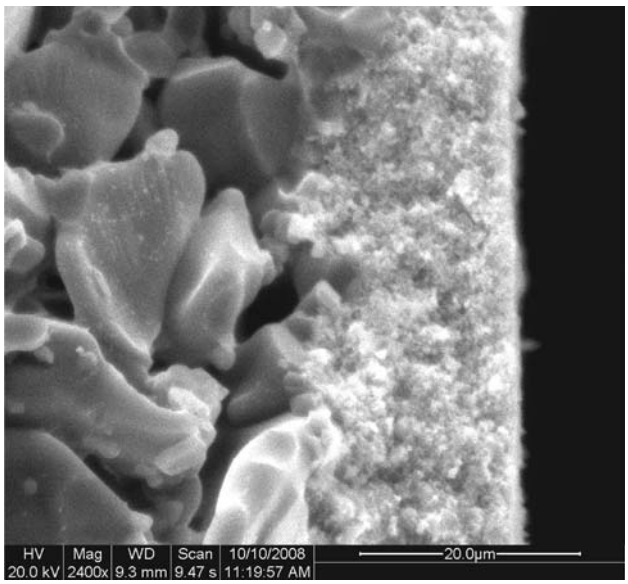

Fig. 4 The cross-section image of α-Al_2O_3 membrane sintered at 1225 °C

heating were performed in air in the range from room temperature to 1450 °C at a heating rate of 2 °C/min.

Characterization of the pore structures

In order to measure the mean pore diameters of the unsupported and supported membranes, a gas permeation technique [31, 32] was used. The mean pore size can be correlated to the following equation:

$$r = \frac{8.48 \cdot \mu \cdot \sqrt{R_g T}}{\sqrt{M}} \times \frac{\beta}{\alpha} \tag{16}$$

where r is the average pore radius, T is the temperature, M and μ are the molecular weight and viscosity of the permeating gas, respectively, and R_g is the gas constant, α and β represent the pure Knudsen diffusion contribution and pure Poiseuille flow contribution, respectively. β/α can be obtained by fitting the permeance (F/L) and mean pressure P_{av} according to Eq. 17:

$$F/L = Q/S(P_h - P_l) = \alpha + \beta P_{av} \tag{17}$$

where Q is the molar gas flux rate, S is the permeation area of the membrane, and P_h and P_l are the pressures at the high-pressure and low-pressure sides of the membrane, respectively. For unsupported membrane, mean pore size can be obtained directly by fitting the gas permeation data and the average pressure across membrane. For supported membrane, however, the mean pore size measured by the two-layer structure is a summation of the contribution from both support and membrane layer [33]. We use a subtraction method [32, 34, 35] to determine the values of β and α for the membrane layer and obtained corresponding pore size.

The porosity of the unsupported membrane was measured by Archimedes' method. The microstructures of the membranes were observed by scanning electron microscopy (SEM) (Quanta 200, Philip, USA). The permeability of the supported membrane was measured by pure water flux (PWF) in across-flow filtration.

Results and discussions

Shrinkage characteristics of α-alumina

In order to calculate the porosity and pore size, the shrinkage behavior during sintering was evaluated by thermal dilatometer curve. The shrinkage (ε) and shrinkage rate ($\dot{\varepsilon}$) curves of an unsupported α-alumina membrane in the range 400–1400 °C are shown in Fig. 5. The shrinkage can be considered as the isotropic free shrinkage in all three directions because the "green" unsupported membrane is the bulk material which prepared by alumina particles with high sphericity and narrow particle size distribution. As shown in Fig. 5, the initial sintering is observed at 950 °C. The shrinkage rate increased at about 900 °C and reached a maximum at around 1300 °C with the value of -2.2×10^{-5} s^{-1}.

For the constrained sintering, the constrained shrinkage characteristics in the z-direction cannot be measured directly. However, on the basis of the theory of stress [19], the shrinkage rate in the z-direction can be expressed as follows:

$$\dot{\varepsilon}_z = (1+N)\dot{\varepsilon}_f/(1-N) \tag{18}$$

where N represents the viscous Poisson's ratio, which is a function of the relative density (ρ_r) according to $N = 1/2(\rho_r/(3-2\rho_r))^{1/2}$ [36]. Here, ρ_r can be calculated from the dilatometer data (Fig. 5). In Fig. 6, the shrinkage rate ($\dot{\varepsilon}$) in the z-direction is shown as a function of temperature

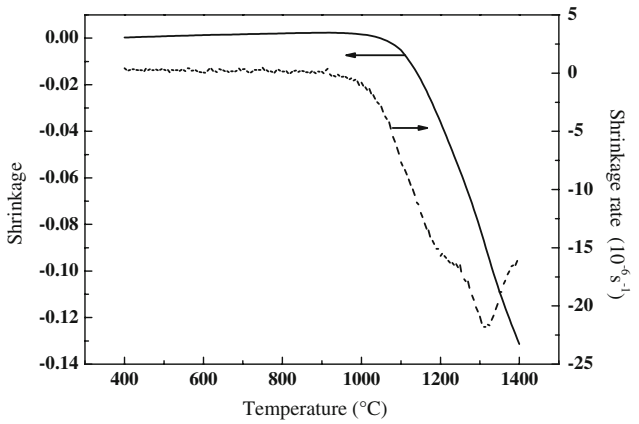

Fig. 5 Dilatometer results of the alumina green body during sintering at the heating rates of 2 °C/min in air atmosphere

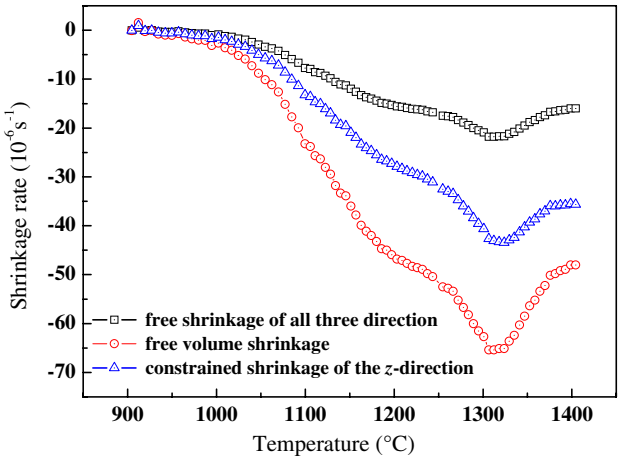

Fig. 6 Shrinkage rate in z direction as a function of temperature for free sintering and constrained sintering

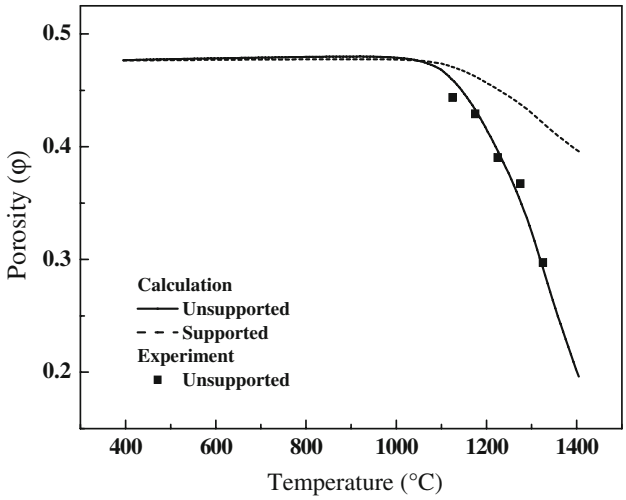

Fig. 7 Porosity changed with temperature of the unsupported and supported membranes

for the case of constrained sintering. The experimental results of free sintering were also included for comparison. In the case of constrained sintering for the supported membrane, with zero-shrinkage in the plane of the membrane, the shrinkage rate perpendicular to the membrane (z-direction) is faster than the free linear shrinkage rate. The maximum shrinkage rate in the z-direction attains a value of -4.3×10^{-5} s^{-1}, which is twice of that for free sintering. However, the volume shrinkage rate ($\Delta \dot{V}/V$) is the sum of the three linear shrinkage rates for the unsupported membrane, and is the shrinkage rate in the z-direction for the supported membrane. Thus, constraint reduces the rate of volume change during sintering and in turn affects the pore structures of supported membranes.

Model prediction for porosity

With the measured shrinkages (ε) in Fig. 5, the trend of porosity varying with temperature for unsupported and supported membranes can be calculated from Eqs. 6 and 12. The calculated results are shown in Fig. 7. For the unsupported membranes, the calculated porosity decreased from 0.47 for the membrane sintered at 1000 °C to 0.2 for that sintered at 1400 °C. These calculated results are in reasonable agreement with the experimental data measured by Archimedes' method, as shown in Fig. 7. It indicates that the proposed model is suitable to quantitatively predict porosity of unsupported membranes.

Since the porosity in membrane layer was difficult to measure in situ for supported membranes, the value was estimated from the corresponding unsupported membrane treated under the same condition by mercury porosimetry [15]. However, it is unreasonable because the restricting effect of support on the membrane layer generates no distortion in parallel membrane surface, but leads to shrinkage only in the perpendicular direction. And this difference in shrinkage behavior in turn produces different microstructure changes during sintering process from that of unsupported membrane. Thus, from Fig. 7, it is indicated that the predicted porosity of a supported membrane is higher than that of an unsupported membrane sintered at the same temperature, and this difference is accentuated with increasing temperature. Considering the constraint exerted by the substrate, volume diminution is lower compared with unsupported membranes. Therefore, the predicted porosity of the supported membranes shown by a dashed line in Fig. 7 is more reasonable than that based on the results from free sintering (solid line) without considering the constraint imposed by the support.

Model verification and validation

Pore size measured by gas permeation technique

The pore sizes of both unsupported and supported membranes were measured by a gas permeation technique at different average pressures. Figure 8 shows the permeance for unsupported membranes (a) and supported membranes with two-layer composite structure (b) after sintering at the temperature of 1125–1325 °C for 2 h. For unsupported membranes, the permeance data and average pressures can be linearly fitted to obtain α and β according to Eq. 17 and the mean pore size can then be calculated directly from β/α with Eq. 16. For the supported membrane, we firstly measured the permeation data for the support only and obtained the α_s,β_s values of support: $\alpha_s = 6 \times 10^{-5}$ mol m^{-2} s^{-1}Pa^{-1} and $\beta_s = 2 \times 10^{-9}$mol m^{-2} s^{-1}Pa^{-2}. Then using the data in Fig. 8b, the permeance and mean pore size of membrane

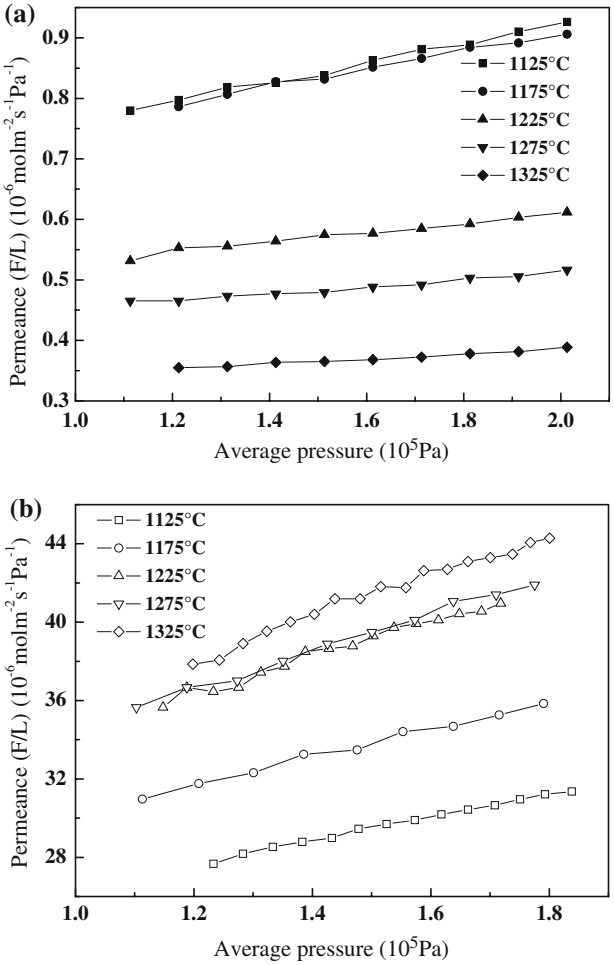

Fig. 8 Gas permeability for **a** unsupported membranes and **b** supported membranes sintered at 1125–1325 °C for 2 h

layer can be obtained by subtracting the effect of support. The resulting coefficients α,β and the mean pore diameters for the unsupported membrane and separation layer of the supported membranes are listed in Table 1. From Table 1, it is clear that the values of α and β for the two membranes are not on the same scale. The difference in the values of α and β between these two series of samples is due to the difference in the thicknesses of the membranes, which are 2.5 mm and 20 μm for the unsupported and supported membranes, respectively. However, the β/α values of the unsupported and supported membranes sintered at the same temperature tend to converge since the effects of membrane thickness on pure Knudsen diffusion (α) and pure Poiseuille flow (β) co-exist in the relevant pressure range. Therefore, the mean pore diameter measured by this gas permeation technique is independent of the membrane thickness, and hence the values obtained reflected the changes in this parameter with the sintering temperature for the two series of samples.

It is also found from Table 1 that the mean pore diameters of the two kinds of membrane are 230 nm and 242 nm, respectively, for the same sintering temperature of 1125 °C. That is to say, the mean pore diameters of the two membranes are very similar after sintering at a lower temperature, indicating the presence of rather similar flow channels. The trends of the mean pore diameters varying with temperature for unsupported and supported membranes were different. As the temperature is increased from 1125 to 1325 °C, the mean pore diameter decreases from 230 nm to 116 nm for the unsupported membrane, whereas it increases from 252 nm to 342 nm for the supported membrane. The reason for this is that the sintering in the unsupported membrane is unconstrained, hence shrinkage occurs uniformly in three directions and the pore diameter decreases continuously. However, for the supported membrane, the shrinkage in the x–y directions is completely constrained by the substrate. Though the shrinkage perpendicular to the membrane is large, it is insufficient to compensate for the smaller volume change due to constraint, resulting in an increase in pore size to make up the

Table 1 Experimental values of α, β, and the mean pore diameters (d) for unsupported and supported membranes with N_2 at room temperature

Membranes	Temperature (°C)	α (10^{-6}mol m^{-2} s^{-1} Pa^{-1})	β (10^{-11}mol m^{-2} s^{-1} Pa^{-2})	α_m (10^{-6}mol m^{-2} s^{-1} Pa^{-1})	β_m (10^{-11}mol m^{-2} s^{-1} Pa^{-2})	d_m (nm)
Unsupported	1125	0.6015	0.1608			230
Unsupported	1175	0.6127	0.1472			206
Unsupported	1225	0.4491	0.0804			154
Unsupported	1275	0.397	0.0573			124
Unsupported	1325	0.3042	0.0408			116
Supported	1125	20.514	5.9611	23.083	6.4287	242
Supported	1175	23.185	7.082	27.641	7.996	252
Supported	1225	25.462	9.106	29.806	10.046	292
Supported	1275	25.219	9.4938	29.547	10.498	308
Supported	1325	25.439	10.581	28.88	11.342	342

difference in volume change of unsupported and supported membranes.

Pore size calculated by the model

The mean pore diameters of unsupported and supported membranes could be calculated by Eqs. 9 and 15 based on the measured shrinkages, predicted porosity and initial particle radius. The results are shown in Fig. 9a. The prediction curves show the similar trend to experimental data. The predicted values are higher than the experimental data at low sintering temperatures since the stacked array of particles is simplified as cubic (the coordination number of each particle is six) and the pores is simplified as cylindrical. In fact, the actual stacking may be more compact than cubic stack. If the coordination number of each particle is eight, the variational trend of pore size relative to temperature is more approximate to the experimental value, as shown in Fig. 9b. Another phenomenon is that compared to the experimental data the calculated values are higher for the unsupported membrane but significantly lower for the supported membrane. The reason may be that the model does not take account of the effect of holding time for membrane sintering, which could increase shrinkage to affect pore size.

The SEM images of supported membranes sintered at different temperatures are shown in Fig. 10. In order to demonstrate the neck contact between membrane particles, and the interface between membrane layer and support, the cross-section images are shown in Fig. 11. As the temperature is increased, neck connection and growth evidently occur, and the porosity decreases and the pore size increases (Figs. 10 and 11). The change of pore size observed is consistent with the experimental data (Table 1) and the predicted results (Fig. 9).

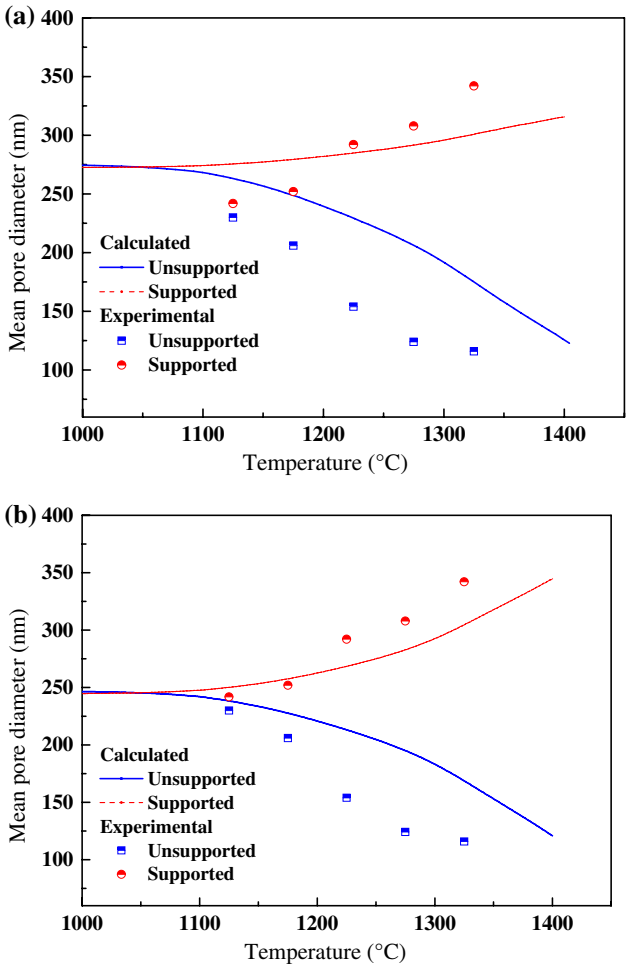

Fig. 9 Comparison of model calculations with experimental data for pore size as a function of sintering temperature. Particle coordination number is **a** six, **b** eight

Water permeability measurements

Figure 12 shows the pure water flux (PWF) of supported membranes sintered at different temperatures. The results show that the supported membrane sintered at a higher temperature had a higher PWF. According to the Poiseuille equation, water flux is related to the mean pore size, porosity, and membrane thickness, and of these three factors pore size seems to be the most pertinent [11]. Thus, the water permeability increases because the pore size of supported membranes increases while the porosity decreases only moderately as the sintering temperature is increased, which is in agreement with the trends predicted by model.

Conclusion

A model has been developed based on the sintering mechanism to calculate the change in the pore size and porosity of a ceramic membrane during sintering process. Combining with the dilatometer results of fabrication material (α-alumina), the pore size and porosity of both unsupported and supported membranes can be predicted by the proposed model. The porosity of the supported membrane is found to be greater than that of the unsupported membrane at the same sintering temperature due to the effect of the rigid substrate. As the sintering temperature is increased, the mean pore size decreases for the unsupported membranes but increases for the supported membranes. Experimental data for unsupported and supported α-alumina membranes have been found to be in good agreement with the prediction results by the model.

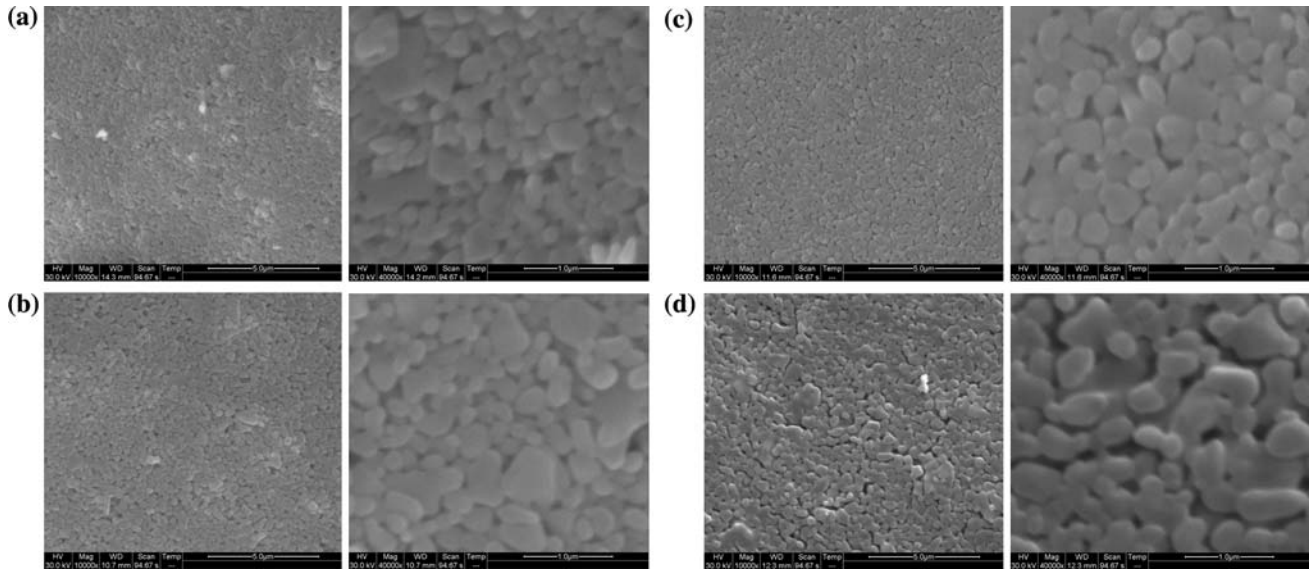

Fig. 10 Surface images of α-Al_2O_3 membranes sintered at **a** 1175 °C, **b** 1225 °C, **c** 1275 °C, and **d** 1325 °C with the magnification of 10,000× and 40,000×

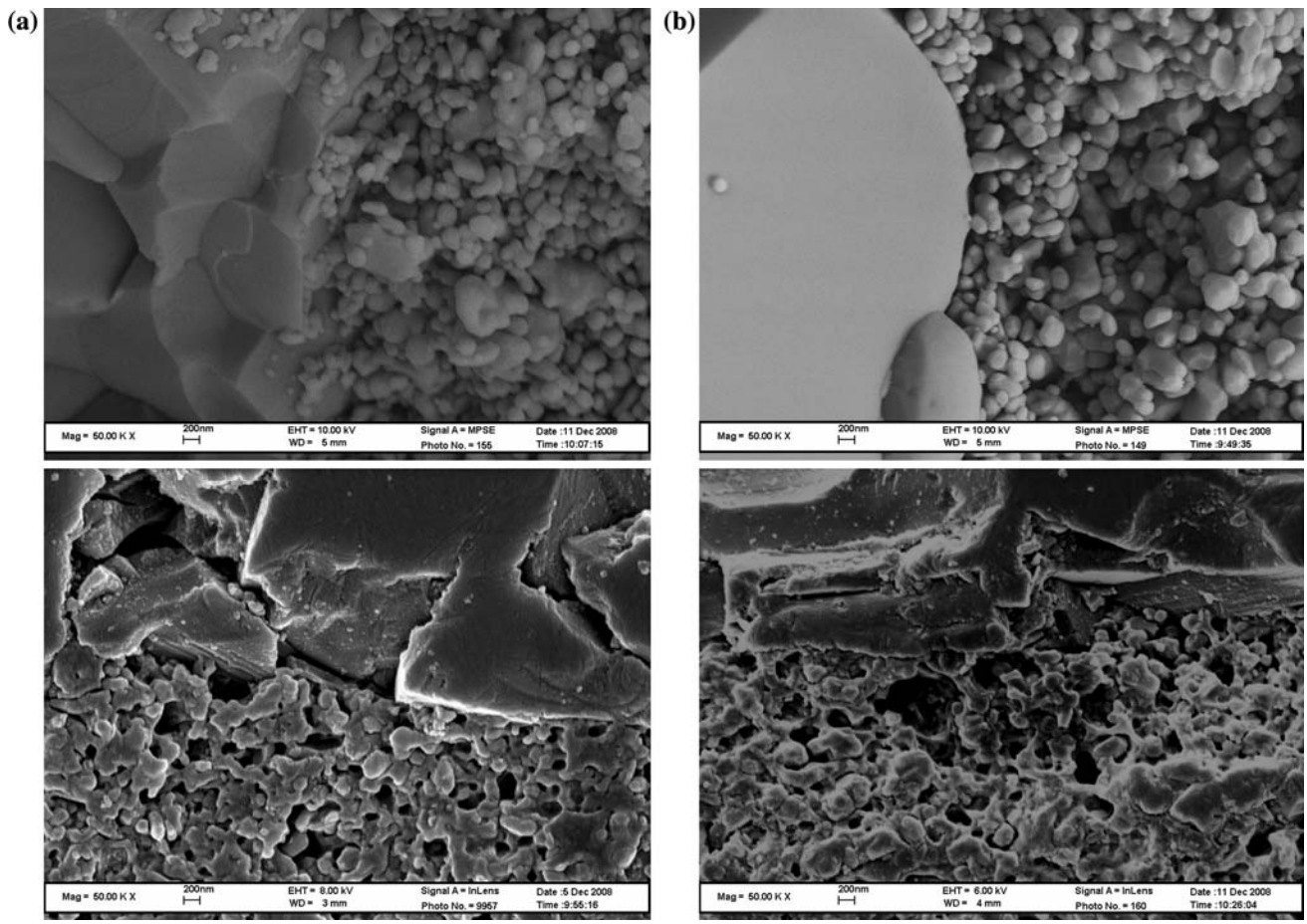

Fig. 11 The cross-section image of α-Al_2O_3 membrane sintered at **a** 1225 °C and **b** 1325 °C

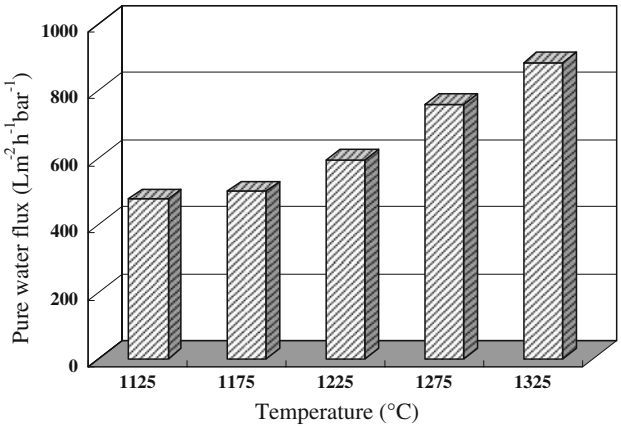

Fig. 12 Pure water flux of supported membranes sintered at different temperatures

Acknowledgements This work was supported by the National Basic Research Program of China (No. 2009CB623400) and the National Nature Science Foundation of China (No. 20436030).

References

1. Burggraaf AJ (1996) Fundamentals of inorganic membrane science and technology. Elsevier Science, Netherlands
2. Shojai F, Mäntylä TA (2001) J Mater Sci 36:3437. doi: 10.1023/A:1017908011672
3. Darcovich K, Toll F, Hontanx P, Roux V, Shinagawa K (2003) Mater Sci Eng A 348:76
4. Whittemore OJ, Sipe JJ Jr (1974) Powder Technol 9:159
5. Kingery WD, Bowen HK, Uhlmann DR (1975) Introduction to ceramics. Wiley, New York
6. Long GG, Krueger S (1991) J Am Ceram Soc 74:1578
7. Ikegami T, Kotani K, Eguchi K (1987) J Am Ceram Soc 70:885
8. Cho J, Chan HM, Harmer MP, Rickman JM (1998) J Am Ceram Soc 81:3001
9. Drahus MD, Chan HM, Rickman JM, Harmer MP (2005) J Am Ceram Soc 88:3369
10. Dillon SJ, Harmer MP (2008) J Eur Ceram Soc 28:1485
11. Wang P, Huang P, Xu NP, Shi J, Lin YS (1999) J Membr Sci 155:309
12. Levänen E, Mäntylä TA (2002) J Eur Ceram Soc 22:613
13. Wallot J, Reynders P, Herzing AA et al (2008) J Eur Ceram Soc 28:2225
14. Guillon O, Krauß S, Rodel J (2007) J Eur Ceram Soc 27:2623
15. Feng J, Fan YQ, Qi H, Xu NP (2007) J Membr Sci 288:20
16. Mohanram A, Lee SH, Messing GL, Green DJ (2006) J Am Ceram Soc 84:1923
17. Nguyen TL, Kobayashi K, Honda T (2004) Solid State Ionics 174:163
18. Garino TJ, Bowen HK (1987) J Am Ceram Soc 70:C315
19. Scherer GW, Garino TJ (1985) J Am Ceram Soc 68:216
20. Garino TJ, Bowen HK (1990) J Am Ceram Soc 73:251
21. Bordia RK, Raj R (1985) J Am Ceram Soc 68:287
22. Carroll DR, Rahaman MN (1994) J Eur Ceram Soc 14:473
23. Bordia RK, Jagota J (1993) J Am Ceram Soc 76:2475
24. Kang SL (2005) Sintering densification, grain growth. Elsevier Science, Netherlands
25. Rahaman MN (2003) Ceramic processing and sintering. Marcel Dekker, New York
26. Akash A, Mayo MJ (1999) J Am Ceram Soc 82:2948
27. Chang JC, Jean JH (2006) J Am Ceram Soc 89:829
28. Tzeng SY, Jean JH (2002) J Am Ceram Soc 85:335
29. Zuo R, Aulbach E, Rodel J (2004) J Am Ceram Soc 87:526
30. Huang CC, Jean JH (2004) J Am Ceram Soc 87:1454
31. Lin YS (1993) J Membr Sci 79:55
32. Lin YS, Burggraaf AJ (1993) J Membr Sci 79:65
33. Yasuda H, Tsai JT (1974) J Appl Polym Sci 18:805
34. Lin YS, Burggraaf AJ (1992) AIChE J 38:445
35. Uhlhorn RJR, Keizer K, Burggraaf AJ (1992) J Mater Sci 27:527. doi:10.1007/BF00543947
36. Scherer JW, Rekhon SM (1982) J Am Ceram Soc 65:352